A&A 409, 1037–1053 (2003)
DOI: 10.1051/0004-6361:20031229

Astronomy & Astrophysics

The pre-main sequence spectroscopic binary AK Scorpii revisited⋆,⋆⋆

S. H. P. Alencar[1,6], C. H. F. Melo[2], C. P. Dullemond[3], J. Andersen[4], C. Batalha[5], L. P. R. Vaz[1], and R. D. Mathieu[7]

[1] Departamento de Física, ICEx-UFMG, CP 702, Belo Horizonte, MG 30123-970, Brazil
e-mail: lpv@fisica.ufmg.br
[2] European Southern Observatory, Casilla 19001, Santiago 19, Chile
e-mail: cmelo@eso.org
[3] Max Planck Institut für Astrophysik, Postfach 1317, 85741 Garching, Germany,
e-mail: dullemon@mpa-garching.mpg.de
[4] Niels Bohr Institute for Astronomy, Physics, and Geophysics, Astronomical Observatory, Juliane Maries Vej 30, 2100 Copenhagen, Denmark
e-mail: ja@astro.ku.dk
[5] Observatório Nacional, Departamento de Astrofísica, Rua General José Cristino 77, São Cristóvão, Rio de Janeiro 20921-400, Brasil
e-mail: celso@on.br
[6] Universidade de São Paulo, IAG, Departamento de Astronomia, Rua do Matão, 1226, São Paulo 05508-900, Brasil
e-mail: alencar@astro.iag.usp.br
[7] Department of Astronomy, University of Wisconsin-Madison, 475 North Charter Street, Madison, WI 53706, USA
e-mail: mathieu@astro.wisc.edu

Received 28 April 2003 / Accepted 28 July 2003

Abstract. We present an analysis of 32 high-resolution echelle spectra of the pre-main sequence spectroscopic binary AK Sco obtained during 1998 and 2000, as well as a total of 72 photoelectric radial-velocity observations from the period 1986–1994. These data allow considerable improvement of the period and other orbital parameters of AK Sco. Our analysis also includes eight series of photometric observations in the *uvby* and Geneva seven-color systems from 1987, 1989, 1990, 1992, 1994 and 1997. No eclipses or other periodic variations are seen in the photometry, but the well-determined HIPPARCOS parallax allows us to constrain the orbital inclination of the system to the range $65° < i < 70°$, leading to the following physical parameters for the two near-identical stars: $M = 1.35 \pm 0.07\ M_\odot$, $R = 1.59 \pm 0.35\ R_\odot$, and $v \sin i = 18.5 \pm 1.0$ km s^{-1}.
Disk models have been fit to the spectral energy distribution of AK Sco from 350 nm to 1100 μm. The above stellar parameters permit a consistent solution with an inner rim temperature of 1250 K, instead of the usual 1500 K corresponding to the dust evaporation temperature. Dynamical effects due to tidal interaction of the binary system are supposed to be responsible for pushing the inner disk radius outwards. Combining simultaneous photometric and spectroscopic data sets allows us to compute the dust obscuration in front of each star at several points over the orbit. The results demonstrate the existence of substructure at scales of just a single stellar diameter, and also that one side of the orbit is more heavily obscured than the other.
The spectrum of AK Sco exhibits emission and absorption lines that show substantial variety and variability in shape. The accretion-related lines may show both outflow and infall signatures. The system displays variations at the binary orbital period in both the photospheric and accretion-related line intensities and equivalent widths, although with appreciable scatter. The periodic variations in the blue and red wing of Hβ are almost 180° out of phase.
We find no evidence of enhanced accretion near the periastron passage in AK Sco as expected theoretically and observed previously in DQ Tau, a similarly young binary system with a mass ratio near unity and an eccentric orbit. The Hα equivalent width displays rather smooth variations at the stellar period, peaking around phases 0.6–0.7, far away from periastron where theory expects the maximum accretion rate to occur.

Key words. stars: pre-main-sequence – stars: binaries: spectroscopic – stars: formation – stars: individual: AK Sco – line: profiles

Send offprint requests to: S. H. P. Alencar,
e-mail: silvia@fisica.ufmg.br

⋆ Based on observations obtained at the 0.5-m (SAT) and 1.54-m Danish telescopes and the Swiss 70-cm, Swiss Euler 1.2-m and ESO 1.52-m telescopes at ESO, La Silla, Chile.

⋆⋆ The complete version of Table 3 is only available in electronic form at the CDS via anonymous ftp to cdsarc.u-strasbg.fr (130.79.128.5) or via http://cdsweb.u-strasbg.fr/cgi-bin/qcat?J/A+A/409/1037

1. Introduction

Classical T Tauri stars (CTTSs) are young stars of near-solar mass ($M < 2\ M_{\odot}$). They exhibit a wide variety of permitted and sometimes also forbidden emission lines, together with excess continuum emission that ranges from millimeter to ultraviolet wavelengths. Their spectral energy distribution is consistent with the presence of a circumstellar disk that appears to play a major role in the regulation of the mass flows in the star–disk system. A strong wind component is also thought to be present, producing blueshifted absorption features commonly seen in the Balmer lines. All these features can be generally understood in the framework of a magnetospheric accretion scenario where accreting material leaves the disk following the magnetic field lines that shred the disk at a few stellar radii. The disk is said to be locked to the central star. Several of the spectral features mentioned above can be naturally explained in the disk-lock framework (e.g. Hartmann 1998). Stellar angular momentum evolution is also profoundly linked to the star/disk interaction (e.g. Bouvier et al. 1993; Edwards et al. 1993; Bouvier 1997; Bouvier et al. 1997; Allain et al. 1997).

In a binary system, disks can surround the individual components (circumstellar disks) as well as the binary system as a whole (circumbinary disk). From a theoretical point of view, it is believed that dynamical interactions due to tidal and resonant forces will open gaps between the circumstellar disks and the circumbinary disk, preventing the flow of material from the circumbinary to the circumstellar disk(s) (Artymowicz & Lubow 1994). In fact, modeling of the observed Spectral Energy Distributions (SEDs) of different binary systems (Jensen & Mathieu 1997) and disk images such as those of GG Tau (see Krist et al. 2002, and references therein) point to the presence of gaps in circumbinary disks.

Accretion is known to occur in binary systems at the same level as in single stars, regardless of the separation between the components (Mathieu 1994). In spectroscopic binaries with periods of a few days, the components are too close to allow for the existence of circumstellar disks around the individual stars, suggesting that matter is probably being accreted directly from a circumbinary disk. How this might occur is, however, an open question. Artymowicz & Lubow (1996) have shown that under special circumstances, a flow of matter can occur in the form of time-dependent gas streams. According to their calculations, in the case of binary systems with mass ratios near one and eccentric orbits ($e \sim 0.5$), the mass transfer rate would reach a maximum at orbital phases 0.8–1.15, i.e. near periastron. Mathieu et al. (1997) and Basri et al. (1997) have shown that in the binary system DQ Tau, both spectroscopic and photometric variations indicate that the system is very likely experiencing episodes of pulsed accretion near the periastron passage. Brigthenings, as well as periodic variations of veiling and Hα strength are observed to be in phase with the orbital motion. The agreement between theory and observations in the special case of DQ Tau is surprisingly good.

In order to test this scenario in another well-observed eccentric binary system, we have undertaken a reanalysis of the Pre-Main Sequence (PMS) spectroscopic binary AK Sco (HD 152404; F5IVe; $V_{\max} = 8.9$), which became known as a pre-main sequence star when Herbig & Rao (1972) discovered strong Hα emission and Li I absorption lines in its spectrum. Later, Andersen et al. (1989) showed that AK Sco is actually a double-lined spectroscopic binary of short period (13.6 days) and large eccentricity ($e = 0.47$). No evidence for eclipses could be found in the photometry then available in the literature. Their suggestion that AK Sco belongs to the Upper Sco star formation region seems confirmed by the Hipparcos distance, $D = 145^{+38}_{-25}$ pc, which is consistent with that of Upper Sco (de Zeeuw et al. 1999).

Andersen et al. (1989) fit the infrared SED of AK Sco with a simple model consisting of two blackbody dust components. Their temperatures (1700 K and 170 K) and dimensions could be plausibly interpreted in terms of matter bound to the binary system plus a protoplanetary cloud. A more modern model was fit by Jensen & Mathieu (1997), who used a geometrically thin disk with a power-law surface-density distribution and a hole to simulate disk clearing by the binary. In order to fit the near-infrared region and silicate emission in AK Sco they had to include a small amount of optically thin material inside the hole, indicating that AK Sco is not very efficient at clearing the disk gap. Their result does not preclude a dynamically cleared region near the star, but suggests some continued replenishment of the expected disk gap.

Given its combination of an apparently classical binary orbit of high eccentricity with several of the spectral and photometric attributes of CTTSs, AK Sco should offer a favorable opportunity to shed light on these fundamental questions. We have therefore obtained considerable amounts of new spectroscopic and photometric data for AK Sco and discuss in the following the information they provide on the nature of the system and the relationships between the flow of accreting matter and the binary nature of AK Sco.

2. New observations of AK Sco

2.1. Spectroscopy

Finding eclipses in AK Sco would obviously greatly improve our knowledge of the physical parameters of the system. The 1986–1988 photoelectric radial-velocity observations discussed by Andersen et al. (1989) were therefore continued in 1989–1994 in order to refine the period and spectroscopic orbital elements of AK Sco and allow precise prediction of possible times of eclipse. Combined with simultaneous photometry, these data also allow to determine the amount of obscuring matter in front of each individual star at each point of the orbit. Altogether, CORAVEL radial velocities, usually for both stars, are now available for a total of 72 epochs during the period 1986–1994.

In order to study the line profile variations of AK Sco in more detail, we also obtained high-resolution spectra of the system in 1998 and 2000 with the Swiss 1.2 m Euler telescope and CORALIE echelle spectrograph (Baranne et al. 1996; Queloz et al. 2000), and in 2000 with the ESO 1.52-m telescope and FEROS echelle spectrograph (Kaufer & Pasquini 1998; Kaufer et al. 2000), both at ESO, La Silla, Chile. FEROS covers the wavelength range 3500 Å–9200 Å at a mean

Table 1. New spectroscopic observations of AK Sco. HJD is the Heliocentric Julian Date (−2 400 000), ϕ the orbital phase of the observation, v_A and v_B are the radial velocities and $(O-C)_A$ and $(O-C)_B$ the corresponding velocity residuals for components A and B, respectively. Sources: 1 = CORAVEL, 2 = CORALIE, 3 = FEROS. The asterisk (∗) symbols mark residuals deviating more than three standard deviations from the theoretical fit (see Fig. 4).

HJD	ϕ	v_A	v_B	O−C A	O−C B	Source	HJD	ϕ	v_A	v_B	O−C A	O−C B	Source	HJD	ϕ	v_A	v_B	O−C A	O−C B	Source
46 652.502	0.8632	−23.44	19.37	−1.27	0.87	1	47 664.779	0.2437	19.01	−23.80	0.54	−1.11	1	49 165.756	0.5330	30.88	−37.29	−0.34	−1.68	1
46 654.628	0.0194		86.31		−0.49	1	47 665.787	0.3177	26.94	−32.04	−0.07	−0.70	1	49 166.720	0.6038	27.41	−31.42	−0.57	0.91	1
46 667.555	0.9693	−88.45		0.57		1	47 666.800	0.3922	31.65	−34.82	0.54	0.67	1	49 167.682	0.6745	25.20	−26.52	3.15	−0.20	1
46 668.566	0.0436	−71.15		1.17		1	47 667.875	0.4711	32.57		0.34		1	49 168.699	0.7492		−9.31		6.3∗	1
46 668.574	0.0442		68.51		−0.33	1	47 667.889	0.4722		−37.44		−0.81	1	49 169.753	0.8266		−0.24		−4.3∗	1
46 669.580	0.1181	−21.26	14.24	−1.95	−1.36	1	47 668.756	0.5359	29.62		−1.51		1	49 170.717	0.8975	−39.40	35.53	0.81	−1.25	1
46 670.532	0.1880		−2.87		8.2∗	1	47 668.770	0.5369		−33.66		1.83	1	49 172.660	0.0403	−72.60		2.41		1
46 686.501	0.3614	28.04	−34.13	−1.79	0.07	1	47 669.751	0.6090	28.56		0.91		1	49 172.666	0.0407		70.01		−1.68	1
46 687.501	0.4349		−35.46		1.01	1	47 669.759	0.6096		−31.00		0.95	1	49 175.684	0.2624	22.08	−24.51	0.87	0.95	1
46 687.511	0.4356	33.32		1.24		1	47 670.754	0.6827		−25.58		−0.18	1	49 510.671	0.8767	−27.48	26.15	1.20	1.05	1
46 688.563	0.5129	31.72	−34.66	0.00	1.46	1	47 670.768	0.6837	21.35				1	51 003.758	0.5863	29.26	−33.73	0.26	−0.37	2
46 690.553	0.6592	24.42	−28.76	0.81	−0.86	1	47 671.777	0.7579		0.06		14.0∗	1	51 004.730	0.6577	24.54	−28.50	0.79	−0.46	2
46 691.598	0.7359	12.43	−20.42	−1.34	−2.50	1	47 672.779	0.8315		−0.74		−6.4∗	1	51 005.747	0.7324	14.62	−18.78	0.28	−0.27	2
46 693.547	0.8791	−30.54	27.46	−0.62	1.10	1	47 673.864	0.9112	−50.68		−1.78		1	51 006.819	0.8112	−2.83	0.76	0.19	1.67	2
46 694.569	0.9542	−78.13		1.45		1	47 673.871	0.9117		46.96			1	51 007.699	0.8759	−27.86	24.13	0.38	−0.52	2
46 694.578	0.9549		77.45		0.30	1	47 674.797	0.9798	−95.14		−1.36		1	51 009.583	0.0143	−92.56	90.05	−0.38	0.59	2
46 695.551	0.0264	−85.59		−0.30		1	47 674.826	0.9819		91.70		−0.10	1	51 010.742	0.0995	−30.83	27.50	−0.89	1.13	2
46 695.560	0.0271		83.30		1.28	1	47 674.852	0.9838	−95.27		−0.21		1	51 011.681	0.1685	−3.07	−0.38	−4.5∗	5.0∗	2
46 696.554	0.1001	−29.96	26.47	−0.40	0.48	1	47 675.721	0.0477	−66.87		2.11		1	51 012.800	0.2507	20.15	−22.94	0.60	0.84	2
46 716.509	0.5664	30.17	−32.49	0.19	1.87	1	47 675.730	0.0483		65.61		0.22	1	51 013.711	0.3176	27.23	−31.20	0.23	0.13	2
46 717.503	0.6394	26.77		1.38		1	47 676.748	0.1231		10.21		−2.79	1	51 648.766	0.9804	−94.12	94.00	−0.10	2.68	3
46 717.520	0.6406		−25.95		3.64	1	48 014.806	0.9631	−85.32		0.07		1	51 652.791	0.2761	22.67	−27.04	−0.26	0.16	3
46 718.514	0.7137	17.94	−22.89	0.75	−1.50	1	48 014.827	0.9646		81.22		−2.31	1	51 653.744	0.3462	28.64	−32.90	−0.35	0.45	3
46 723.512	0.0809		40.21		1.12	1	48 016.835	0.1121	−23.87	19.02	−1.37	0.19	1	51 654.905	0.4315	30.19	−35.92	−1.83	0.51	3
46 723.522	0.0817	−42.50				1	48 027.713	0.9114	−50.20		−1.14		1	51 655.760	0.4943	32.33	−35.97	0.29	0.47	3
46 724.524	0.1553		−1.90		−1.06	1	48 028.816	0.9925	−96.14		0.42		1	51 656.781	0.5693	33.01	−32.34	3.16	1.88	3
46 725.511	0.2278	15.24	−20.99	−0.54	−1.03	1	48 028.826	0.9932		92.03		−1.91	1	51 664.861	0.1630	5.56	−8.00	6.0∗	−4.44	2
46 837.828	0.4807	32.14		−0.04		1	48 029.759	0.0618	−60.87		−3.53		1	51 665.827	0.2340	17.46	−18.88	0.57	2.20	2
46 837.837	0.4813		−36.68		−0.10	1	48 029.771	0.0627		54.96		1.55	1	51 666.870	0.3107	26.67	−30.87	0.24	−0.12	2
46 839.837	0.6283	26.49		0.22		1	48 783.705	0.4605	30.36	−37.38	−1.88	−0.73	1	51 667.892	0.3858	26.66	−35.34	−4.22	−0.07	2
46 839.845	0.6289		−29.53		1.02	1	48 784.688	0.5327	28.86	−34.90	−2.36	0.72	1	51 669.906	0.5338	31.85	−35.47	0.66	0.11	2
46 979.769	0.9103		46.25		1.30	1	48 785.693	0.6066	26.13	−32.36	−1.67	−0.21	1	51 670.907	0.6073	28.47	−30.97	0.71	1.13	2
46 980.748	0.9822		93.00		1.10	1	48 786.849	0.6915	22.42	−25.72	2.31	−1.37	1	51 671.910	0.6810	21.13	−25.25	−0.20	0.34	2
46 980.759	0.9830	−94.93		−0.10		1	48 788.713	0.8285		0.70		−3.93	1	51 672.935	0.7563	8.42	−15.09	−1.70	−0.86	2
47 042.531	0.5219		−34.95		0.96	1	48 789.705	0.9013	−42.08		0.49		1	51 674.907	0.9012	−42.32	40.75	0.14	1.69	2
47 042.542	0.5227	32.78		1.28		1	48 789.713	0.9019		35.75		−3.80	1	51 676.901	0.0477	−69.89	68.23	−0.96	2.34	2
47 044.553	0.6705	22.25	−26.99	−0.23	−0.24	1	49 158.838	0.0246	−86.66		−0.22		1	51 683.904	0.5623	29.67	−37.28	−0.49	−2.74	2
47 047.494	0.8866	−33.85		0.06		1	49 158.846	0.0252		82.32		−0.93	1	51 684.885	0.6344	25.92	−31.56	0.12	−1.44	2
47 047.506	0.8875		30.20		−0.70	1	49 159.644	0.0839		36.27		−0.68	1	51 685.904	0.7092	19.50	−21.91	1.69	0.11	2
47 049.545	0.0373		73.28		−1.14	1	49 160.661	0.1586		−2.52		−0.49	1	51 686.933	0.7849	1.53	−14.73	−2.44	−6.7∗	2
47 049.553	0.0379	−75.69		1.20		1	49 161.650	0.2313	15.87	−20.70	−0.53	−0.11	1	51 688.890	0.9287	−60.89	57.84	0.15	−0.05	2
47 050.535	0.1100	−24.22	21.30	−0.54	1.27	1	49 162.583	0.2998	24.10	−31.12	−1.34	−1.36	1	51 688.924	0.9311	−62.47	59.60	0.37	−0.12	2
47 070.503	0.5772		−35.05		−1.21	1	49 163.669	0.3796	31.42	−35.54	0.77	−0.51	1							
47 070.511	0.5778	30.05		0.61		1	49 164.686	0.4543	32.22	−37.77	−0.01	−1.14	1							

resolution of $\lambda/\Delta\lambda \approx 48\,000$, while the CORALIE spectra cover a shorter spectral range 3690 Å–6900 Å with a resolving power of 47 000, similar to FEROS. Typical CORALIE exposure times and S/N ratios were about 30 min and 40, while for FEROS a 20 min exposure was enough to reach an S/N ratio near 100 in the Hα region.

The reduction of the FEROS spectra was performed by the on-line software, including flatfielding, background subtraction, removal of cosmic rays, wavelength calibration, barycentric velocity correction, and continuum normalization. A similar on-line reduction system exists for CORALIE: after read-out, the spectrum is extracted, flat-fielded and wavelength calibrated, producing a 2D image which is saved on the disk. Cosmic ray cleaning is performed only prior to the cross-correlation (see below). Barycentric correction is applied afterwards directly on the cross-correlation function (CCF) only and not on the spectrum as in the FEROS case.

The CORALIE on-line reduction system (Queloz 1995) cross-correlates the stellar spectrum with a CORAVEL-type numerical mask (Baranne et al. 1979; Queloz 1995) and also performs a Gaussian fit to the CCF. The procedure yields the Gaussian center, giving the radial velocity, the depth of the CCF dip and the width (σ) of the CCF. The typical internal error of the radial-velocity measurements is about 200 m s^{-1} (Covino et al. 2001). FEROS CCFs were computed off-line using the same procedures and mask as the CORALIE on-line reduction system.

Altogether, the 72 CORAVEL observations and 32 high-resolution spectra thus provide 104 radial velocities covering a total span of 5036 days or 371 orbital cycles; these data are listed in Table 1.

Projected rotational velocities ($v \sin i$) were computed using the calibrations given by Melo et al. (2001) for FEROS and by Santos et al. (2002) for CORALIE. The FEROS and CORALIE $v \sin i$ agree very well, giving mean rotational velocities of $v \sin i_A = 18 \pm 1$ km s^{-1} and $v \sin i_B = 19 \pm 1$ km s^{-1}. These values are also in agreement with the previous rotational velocity measurements given by Andersen et al. (1989). We adopt an average $v \sin i$ for both components of 18.5 ± 1.0 km s^{-1}.

2.2. Photometry

After the data discussed by Andersen et al. (1989), eight series of photoelectric photometry of AK Sco have been obtained at

Table 2. Summary of observing periods.

Serie	Epoch (JD−2 440 000.0)	System	Number of nights	Number of observations
1987	6829.8−6884.8	*uvby*	16	54
1989*a*	7587.8−7787.5	Geneva	138	278
1989*b*	7661.9−7676.9	*uvby*	11	336
1989*c*	7692.6−7714.6	*uvby*	17	474
1990	8013.6−8013.8	*uvby*	1	18
1992	8782.5−8788.7	*uvby*	5	28
1993	9135.6−9165.8	*uvby*	18	198
1994	9510.8−9549.8	*uvby*	31	145

Table 3. *uvby* and Geneva photometry of AK Sco obtained between 1987 and 1994 at ESO, La Silla. The first 3 *uvby* observations (SAT, instrumental system, SAO 208122 used as comparison star), obtained in 1993, are shown in the upper part while those in the Geneva system, obtained in 1989 with the Swiss telescope, are shown in the lower part. The complete version of Table 3 is only available in electronic form at the CDS.

HJD− 2 440 000	Δy	$\Delta(b-y)$	Δm_1	Δc_1
9135.56551	−0.367	0.056	0.081	−0.466
9135.57031	−0.363	0.052	0.088	−0.464
9135.57744	−0.360	0.054	0.082	−0.482

HJD− 2 440 000	VM	U	V	B1	B2	V1	G
7587.846	9.219	1.699	0.083	1.104	1.296	0.835	1.110
7588.855	9.450	1.755	0.023	1.112	1.277	0.777	1.031
7590.856	9.451	1.636	0.105	1.085	1.302	0.850	1.130

La Silla, Chile. The data set denoted 1989*a* was obtained in the Geneva photometric system (Golay 1980) with the photometer P7 (Burnet & Rufener 1979) on the 70 cm Swiss telescope; reduction procedures are described by Rufener (1964, 1985). The seven other sets, all in the Strömgren *uvby* system, were obtained in 1987, 1989 (*b* and *c*), 1990, 1992, 1993 and 1994 with the 50 cm Strömgren Automatic Telescope (SAT) and six-channel photometer (Nielsen et al. 1987). The reduction procedure for these data is described by Vaz et al. (1998). The chief characteristics of the observing periods are briefly summarized in Table 2, while the table with the individual photometric data will be available in electronic form at the CDS. Table 3 contains an excerpt of the data.

Figure 1 shows the *y* magnitude differences (instrumental system) between AK Sco and SAO 208122, contained in the complete version of Table 3.

The observed time series and color-magnitude diagrams are shown in Figs. 2 and 3. The irregular light variations in AK Sco are similar to those of Herbig Ae/Be stars (see e.g. Bibo & Thé 1991). The variations are quite large, with brightness changes of up to one magnitude between consecutive nights and globally exceeding 1.5 mag.

In order to check for the presence of eclipses, synthetic light curves were generated to predict the precise times when

Table 4. Orbital parameters and physical elements. T is the time of periastron passage in Heliocentric Julian Days.

Orbital parameters	
P (days)	13.609453 ± 0.000026
T (J.D.)	46 654.3634 ± 0.0086
K_A (km s^{-1})	64.45 ± 0.23
K_B (km s^{-1})	65.32 ± 0.24
γ (km s^{-1})	−1.97 ± 0.10
e	0.4712 ± 0.0020
ω	185.40° ± 0.33°
σ(1 obs.) (km s^{-1})	1.4
Physical elements	
M_B/M_A	0.987 ± 0.005
$a \sin i$ (AU)	0.14318 ± 0.00005
$M_A \sin i^3$ ($M_\odot$)	1.064 ± 0.007
$M_B \sin i^3$ ($M_\odot$)	1.050 ± 0.007

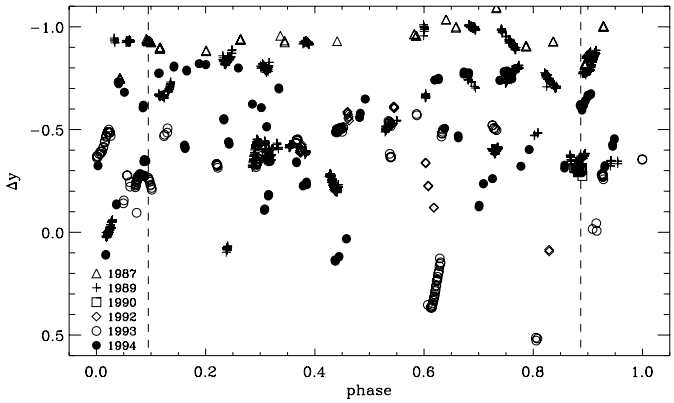

Fig. 1. *y* magnitude differences between AK Sco and SAO 208122 obtained from 1987 and 1994, phased with the spectroscopic ephemeris (i.e. periastron passage at phase 0.0, see Table 4). The dashed lines show the phases when eclipses are expected to occur.

eclipses could occur, combining the spectroscopic orbital elements with a range of assumed inclinations: In orbits of large eccentricity and the orientation seen in AK Sco, the time of light minimum may deviate significantly from the (spectroscopically determined) moment of conjunction. Despite the good coverage of the critical phases, no trace of any eclipses or any other periodic variations was found, showing that the orbital inclination is relatively low (further discussion in Sect. 5).

The color-magnitude diagrams show that the star becomes redder when fainter, as expected for dust obscuration and found also by Andersen et al. (1989). However, considerable scatter and some systematic deviations are seen; e.g., near $V = 9.4$ the magnitude may vary at constant color and vice versa, and occasionally AK Sco even gets bluer in the deepest minima ($V \sim 10$), as is sometimes seen in Herbig Ae/Be stars. The anomalous, steep extinction law characteristic of circumstellar dust with large grains is also seen in the new data, with $R_{b-y} = A_y/E_{b-y} \sim 6$–7 against 4.3 for normal interstellar dust. The non-unique color-magnitude relations suggest that dust with a range of grain sizes and/or other properties is present in the AK Sco system.

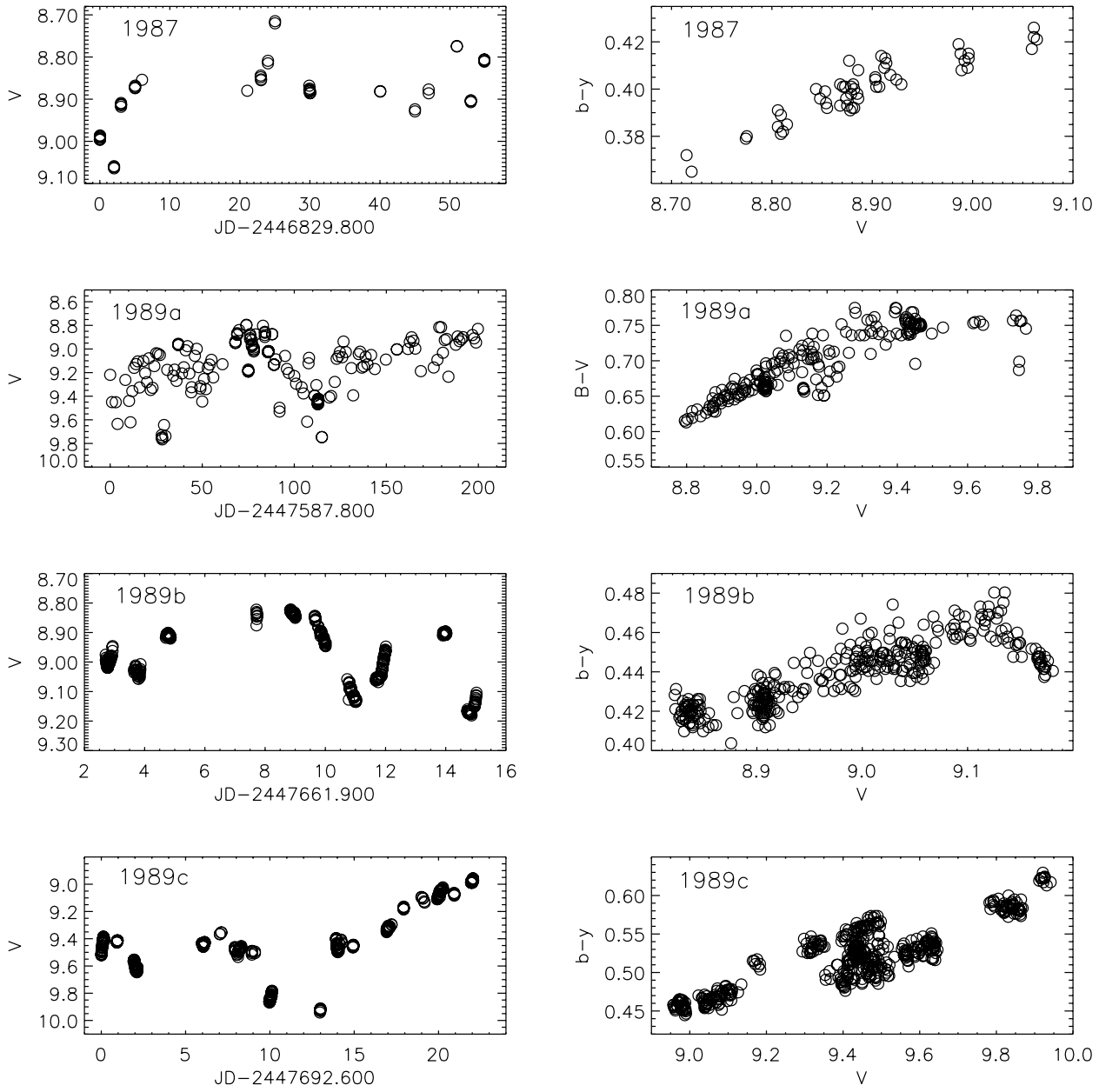

Fig. 2. Light variations and color-magnitude correlations for AK Sco in 1987 and 1989 (data sets 1987, 1989a, 1989b, and 1989c). The system generally becomes redder when fainter, but no unique relationship is observed.

3. Orbital and stellar parameters

3.1. Improved spectroscopic orbital elements

From the radial-velocity data in Table 1 we recompute the spectroscopic orbital elements for both components, using the program SBOP (Etzel 1985). The results are presented in Table 4, and the final orbital solution is shown in Fig. 4. There is good agreement with the elements determined by Andersen et al. (1989), but our errors are substantially smaller. In particular, the error of the period is reduced by a factor 18, due primarily to the longer time base of the data, which allows precise calculations of orbital phases over many years, both past and future.

As a backdrop for the following discussion, we note that the system is seen "side-on", the orbital major axis lying very nearly in the plane of the sky. Any eclipses would be expected to occur at phases 0.098 and 0.886 (for $i = 90°$; 0.095 and 0.886 for $i = 80°$; 0.085 and 0.888 for $i = 70°$), counted from periastron passage as in Fig. 4.

4. Spectroscopic analysis

4.1. Overview of line profiles

Samples of the line profiles observed at different orbital phases and some of the cross-correlation profiles discussed in the following are shown in Fig. 5. Hα is generally in emission and

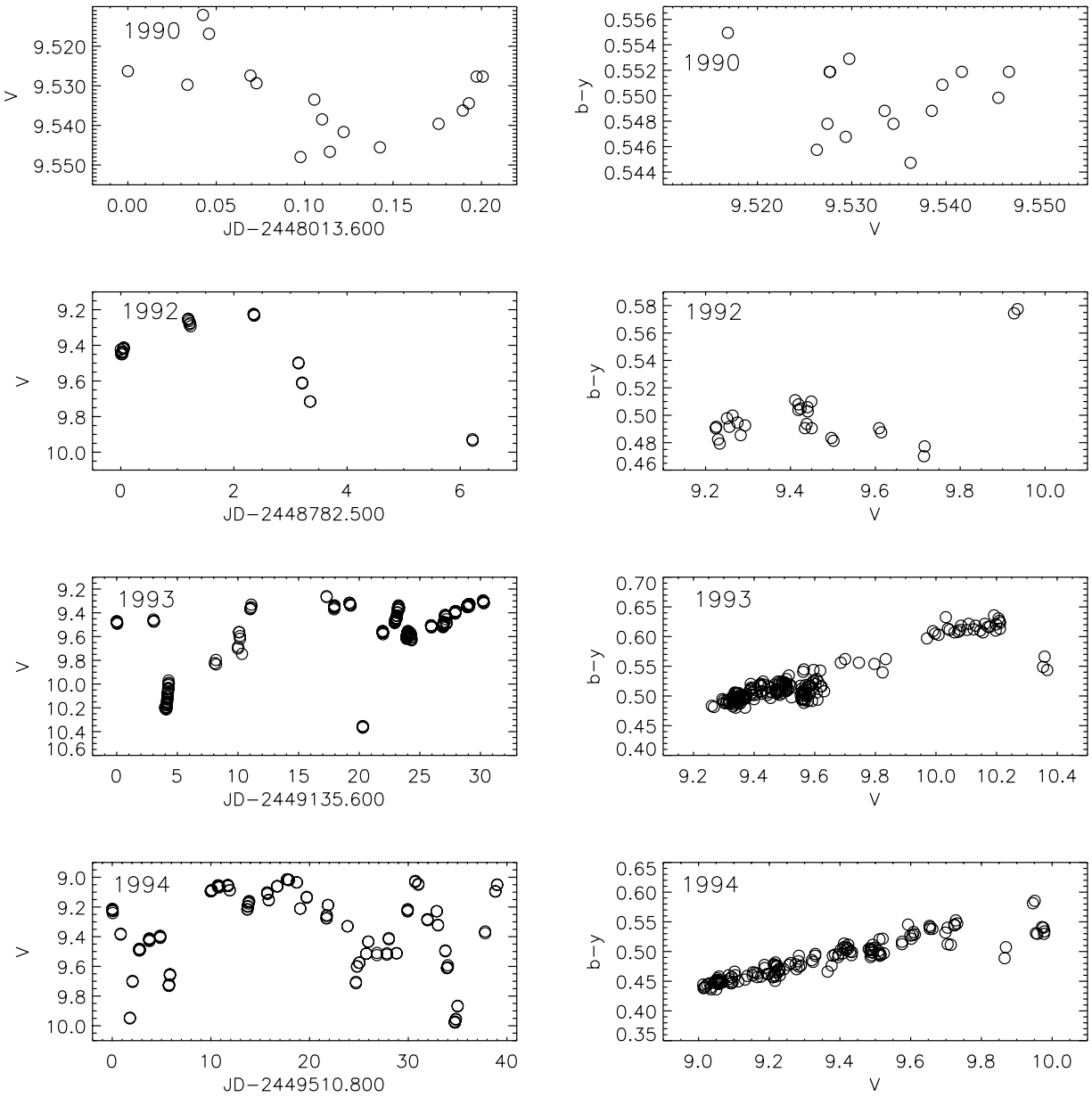

Fig. 3. Light curves and color-magnitude diagrams in four observing epochs (1990, 1992, 1993, 1994). The star generally becomes redder when fainter, but significant deviations from a single-valued relation occur.

may present both blue and red absorptions. Hβ is always in absorption, as expected for F5 stars with hot photospheres in contrast to typical K7-M0 CTTSs, and varies substantially both in the blue and red wings. Spectra taken at phases with large line separations (Figs. 5a,c) clearly show the strong Li lines that indicate the PMS nature of both stars. Figure 5 also includes a sample of NaD and CCF profiles.

Figure 6 shows a sample of Hα profiles corresponding to nearly the same orbital phases, but taken almost two years apart. These profiles clearly differ, but nonetheless present some common characteristics. The spectra close to phase 0.16 present the strongest absorptions in the blue wings among all the observations. In these spectra we clearly see two blueshifted absorptions, one near zero that is also generally present at other phases, and one at higher negative velocities. The spectra close to phase 0.80, on the other hand, present typical mean Hα profiles, with emission in both wings and nearly central absorption. As the stars have the same radial velocity at both phases 0.16 and 0.80, the profile differences cannot be attributed to photospheric line variations. Since no eclipses are observed, the different line profiles at similar stellar radial velocities indicate that the circumstellar environment is not uniform. Most of the line profile variations must be due to accretion and/or outflows since the stellar velocities only reach $\sim\pm94$ km s^{-1} (cf. Fig. 4). Figure 6 shows that these flows vary, both over the orbit and with time, slightly dependent on orbital phase.

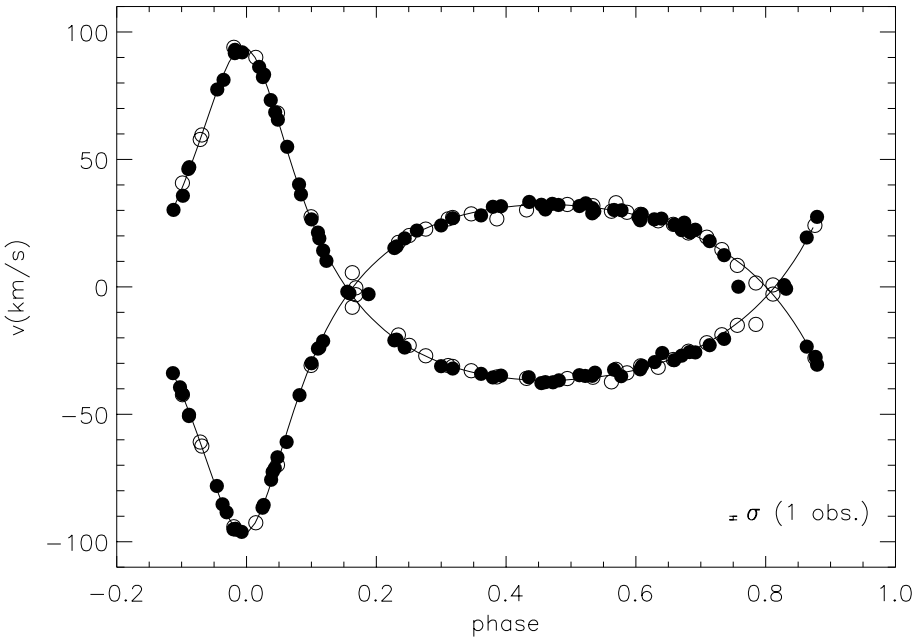

Fig. 4. Radial velocity curve of AK Sco for the orbital solution of Table 4. Filled circles show the CORAVEL measurements; open circles are the FEROS/CORALIE results; star A has its minimum velocity at phase 0.00. The standard deviation of the fit is shown at lower right.

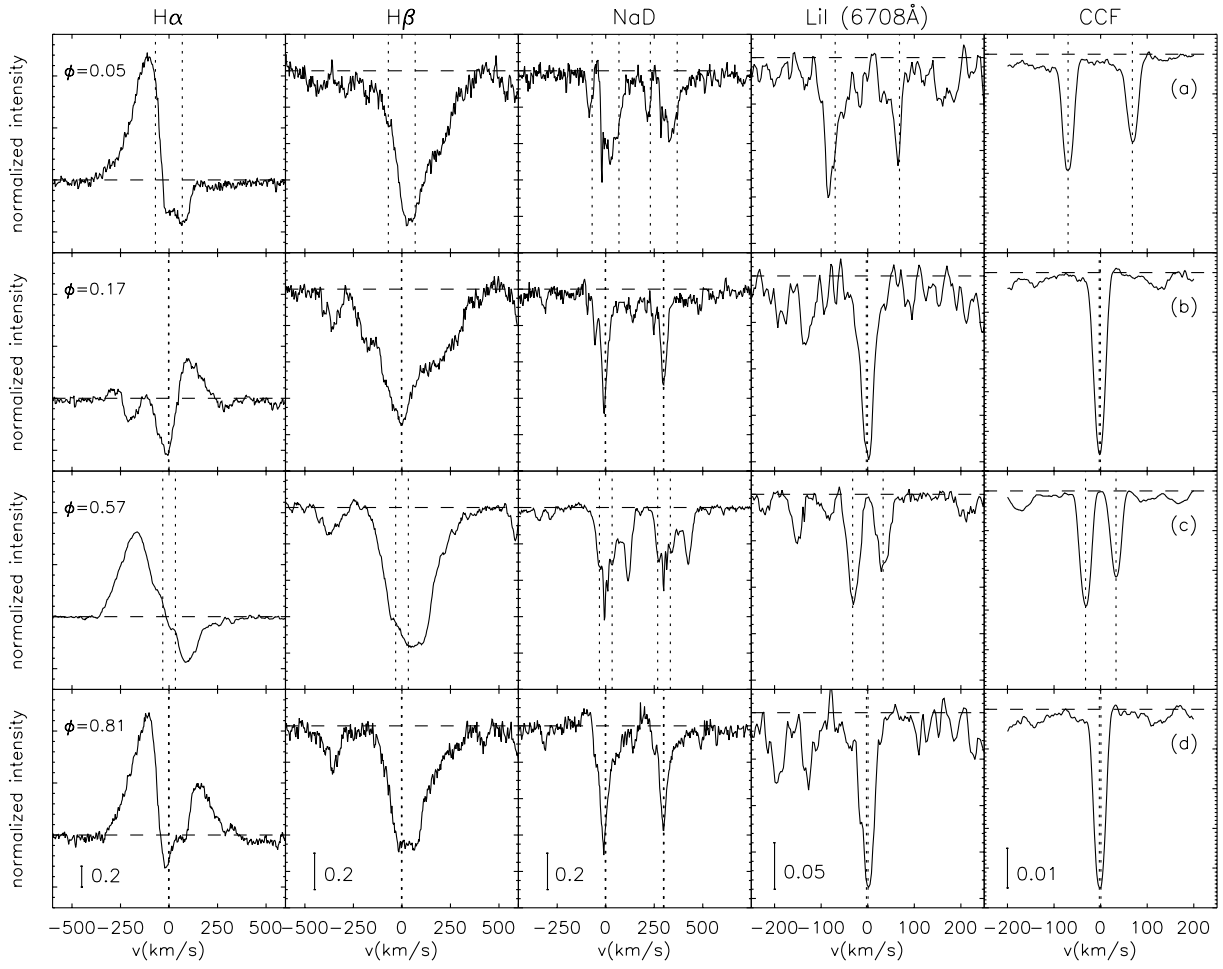

Fig. 5. Samples of spectral line and Cross Correlation Function profiles for different orbital phases. The dotted lines mark the radial velocities of the stars in AK Sco. The dashed line shows the normalized continuum level, and the vertical (intensity) scale of the plots is given in the lower left of each column, in continuum units.

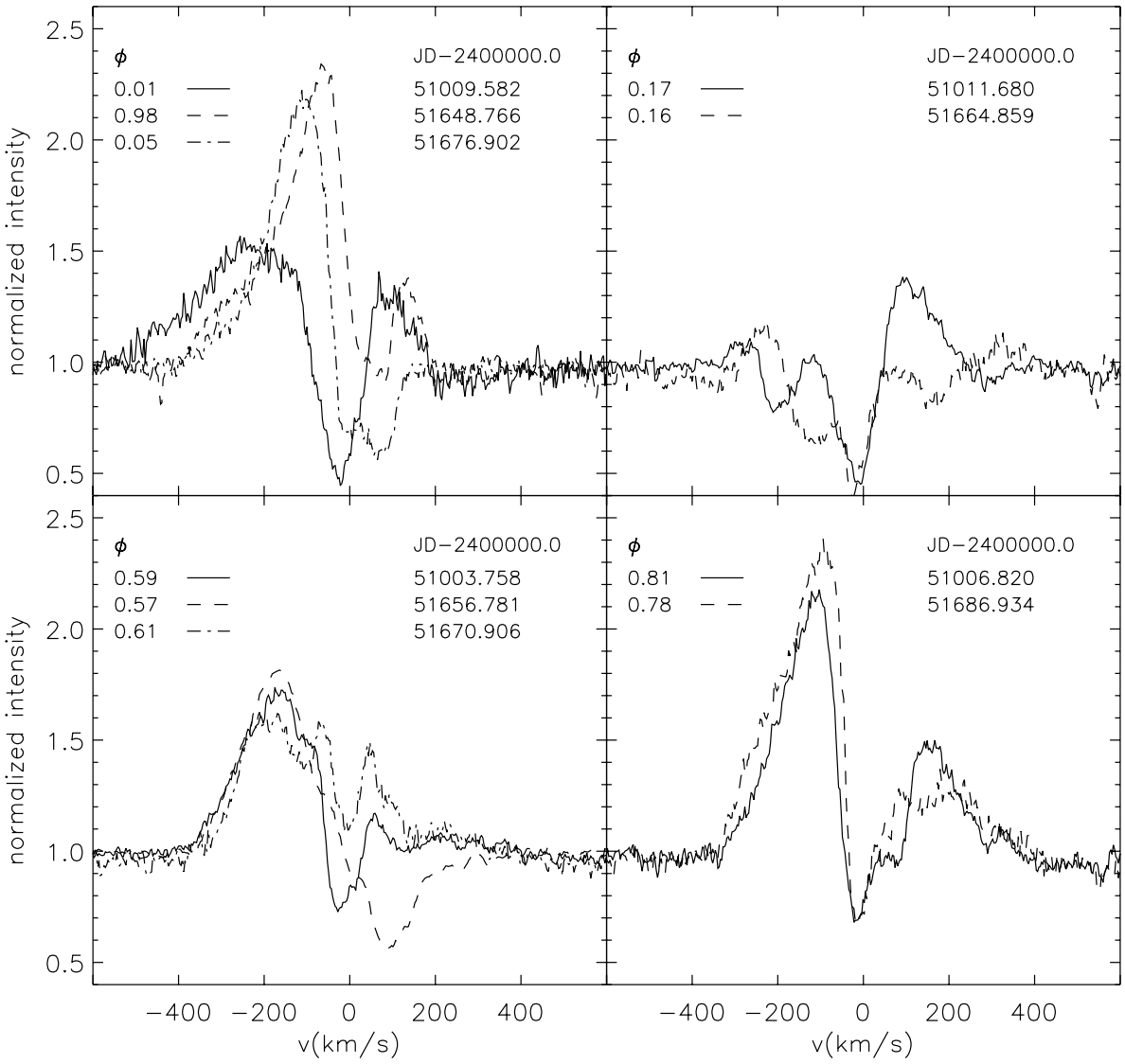

Fig. 6. Hα line profiles observed at similar phases, but almost 2 years apart. The profiles show both remarkable differences and some common characteristics. Each panel shows the phase (ϕ) and Julian date for each profile.

4.2. Photospheric line profiles and Cross Correlation Functions

Individual photospheric lines show low S/N ratios in many of our spectra, so we decided to focus on the CCFs, which represent the mean photospheric profiles. Because the two stars are almost identical, their intrinsic photospheric lines should be equal at all phases. Andersen et al. (1989), however, already noted that while the CCF dips show almost constant width, their depths and thus equivalent widths vary appreciably. They found no systematic variation with orbital phase and suggested that the changes in the CCF profiles as well as the overall brightness variations might be caused by variable obscuration on scales of a few stellar diameters. Some of the CCF variations we observe may be produced on the stars themselves, but if luminosity changes by factors of 2 or more were due to large starspots, one would expect significant spectroscopic changes (e.g. in the excitation temperatures), which have not been seen.

From our larger data set we do find some periodic variations in the CCF strength ratio at the orbital period. Figure 7 shows the CCF depth ratio ($\log(H_B/H_A)$) as a function of orbital phase (ϕ = 0 at the time of periastron passage). Observations with small radial velocity differences were not included, as the separation of their CCF profiles is very uncertain. The CCF changes in 1998–2000 were linked to the orbital motion (cf. Fig. 7), with most of the variations centered near phases 0.3 to 0.5.

It is notable that Andersen et al. (1989) found no similar periodicity. Figure 7 also shows the CCF depth ratio for all the double-lined CORAVEL observations. No periodic variation is apparent in the CORAVEL data, but phases near periastron clearly show the least scatter, while most of the variations occur near phases 0.2–0.5, as in 1998–2000. It is not clear whether the different results for the 1986–1994 and 1998–2000 data are due to the different number of observations, or whether they reflect a true change in the stellar environment (Sect. 6.2).

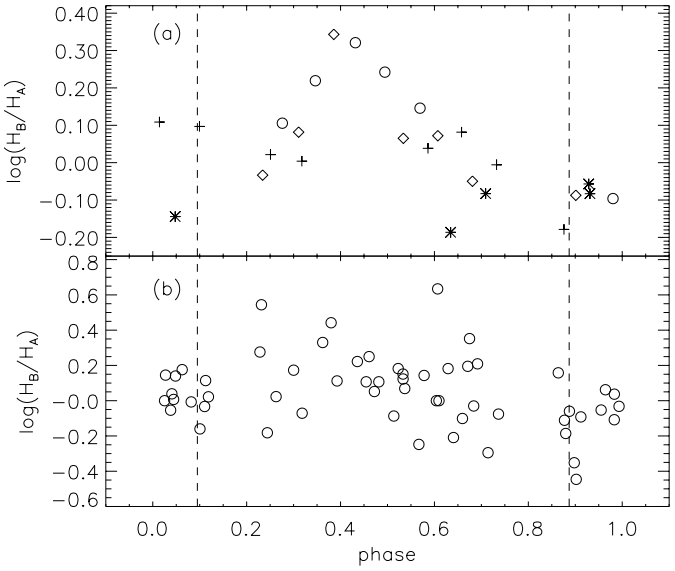

Fig. 7. The CCF depth ratio $\log(H_B/H_A)$ as a function of orbital phase. In panel **a)**, different symbols refer to the different orbital cycles of the 1998–2000 spectra. Panel **b)** shows the CORAVEL data. The dashed lines show the phases when eclipses could occur.

If clumpy dust clouds exist in the disk and/or inside the orbit of the system, the CCF dip ratio will be affected by differential extinction (assuming the stars themselves remain constant). Any dust inside the orbit would on average obscure the star that is most distant ("behind") most strongly, causing its CCF dip to become the shallowest. If, on the other hand, the binary system is located in a clear central region of a thick, clumpy, inclined disk, we would be more likely to have a clear line of sight to the more distant star, leading to the opposite result. Because we know the precise positions of both stars at any given time, we can test these predictions.

Given the adopted component notations and our "side-on" view of AK Sco, star A is seen "in front" from spectroscopic phases 0 to 0.5. Dust inside the system would then weaken the dip of star B, giving a dip ratio $H_B/H_A < 1$ in this phase interval and $H_B/H_A > 1$ in the other half – most markedly around the conjunctions at phases 0.88 and 0.10 (marked by the vertical lines in Fig. 7). If the dust is primarily in a disk outside the system, we would see the reverse.

Figure 7 does in fact show that, in general, $H_B/H_A > 1$ at phases 0.0 to 0.5 and $H_B/H_A < 1$ otherwise, as expected for dust located in a circumbinary disk. But there are also exceptions from the pattern corresponding to an "ideal" disk (e.g. at phases 0.10 and 0.86), indicating a more complicated situation with dust clumps both in a disk and inside the orbit, or perhaps entirely detached from the disk. The structure of the disk is further discussed in Sect. 6.2.

4.3. Accretion related lines

The Balmer line profiles are highly variable (see Fig. 5). We searched for periodic variations in these lines using our spectra from April and May 2000, the only dataset that can be used to study variations with the orbital period (13.61 days), as we have 22 spectra taken over a period of 40 nights. We looked for periodicities in the line's intensities using the Scargle (1982) periodogram estimator as modified by Horne & Baliunas (1986) that is appropriate to handle irregularly spaced data. To evaluate the robustness of the periodicities, we calculated the false alarm probability (FAP) that the peak of each periodicity occurred just by chance and display the FAP as a greyscale in Figs. 8 and 9. Darker regions correspond to lower FAPs, indicating a possible period detection. We found periodicities near the orbital period in the blue wing of Hα and in the blue and red wings of Hβ as shown in Figs. 8 and 9. We show in Fig. 10 the mean Hα and Hβ profiles from April and May 2000; the dashed lines show the regions that presented the above periodicities. It is not easy to associate the periodic regions in Hβ to a specific structure of the line as will be discussed further on. Also shown as shaded areas are the normalized variance profiles as defined by Johns & Basri (1995a), which measure the amount of variability of each velocity bin in the line.

We calculated the equivalent widths of the Hα and Hβ line profiles. The total Hα equivalent width also displays variations at the orbital period (with some scatter, see Fig. 11), while the total Hβ line equivalent width does not. Instead of trying to decompose the Hβ line, we calculated the equivalent width of the different regions of the line profile that displayed the periodic variabilities presented in Fig. 9. Both regions show periodic equivalent width variations near the orbital period with about the same amplitude, but nearly 180° out of phase (see Fig. 12), which explains the lack of periodicity of the total line equivalent width. The low-velocity Hα region that displays periodicities (part of the blue absorption) varies in phase with the Hβ blue wing and consequently out of phase with the Hβ red-wing periodical region.

It is not straightforward to associate each region of Hβ with any given process, like accretion or outflow, since the broad photospheric, accretion and outflow components of both stars superimpose to form the total line profiles. However, comparing the Hβ and NaD profiles, we see in Fig. 13 that when the Hβ line is most redshifted, the NaD lines also exhibit an extra redshifted absorption component at high velocities. These components cannot be associated with the photospheric variations and are clearly visible in the NaD lines because they are much narrower than the Balmer lines, making it possible to distinguish the different contributions to the observed profiles.

Redshifted absorptions at high velocities are generally associated with infall of material; hence we infer that the red wing of Hβ shows signatures of infalling material in the magnetosphere. The blue region of the Hβ line presenting periodicities is located at low velocities and varies in phase with the blue absorption wing of Hα . This could be partly due to winds, in which case infall and outflow components would be out of phase in the Hβ line of AK Sco. This is in fact what was observed by Johns & Basri (1995b) when analysing the profile variations of the CTTS SU Aur. They invoked a magnetospheric accretion model with an inclined dipole field in order to explain the phase lag of the Hβ line variabilities. Due to the inclination of the dipole with respect to the stellar/disk rotation axis, accretion and outflow are favored in opposite phases.

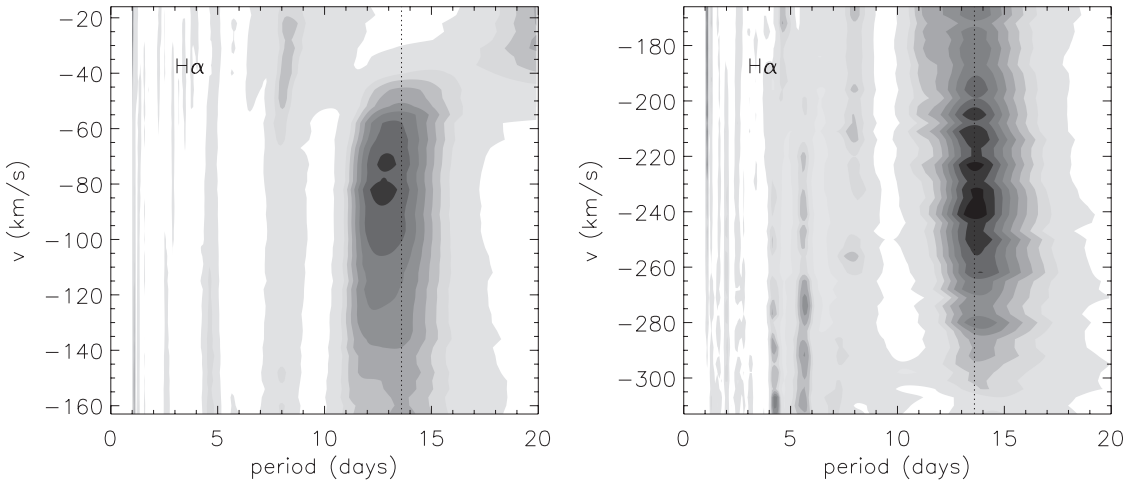

Fig. 8. Hα line regions showing periodicities in the 2000 spectroscopy. The false alarm probability (FAP) that the peak of each periodicity occurred just by chance is shown as a greyscale. The dotted line marks the orbital period (13.61 days). *Left*: maximum power of the periodogram is 6.9 at $v = -82$ km s^{-1}, period = 12.685 days (FAP = 0.02). *Right*: maximum power of the periodogram is 5.9 at $v = -241$ km s^{-1}, period = 13.635 days (FAP = 0.05).

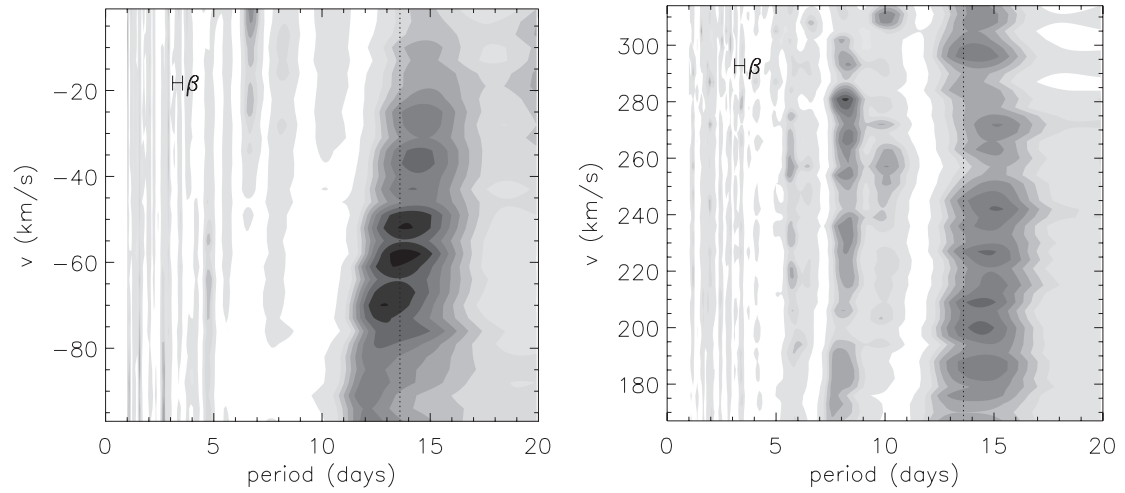

Fig. 9. Hβ line regions showing periodicities in the 2000 spectroscopy. The false alarm probability (FAP) that the peak of each periodicity occurred just by chance is shown as a greyscale. The dotted line marks the orbital period (13.61 days). *Left*: maximum power of the periodogram is 5.8 at $v = -58$ km s^{-1}, period = 13.825 days (FAP = 0.06). *Right*: main power peaks of the periodogram are 6.7 at $v = 281$ km s^{-1}, period = 8.220 days (FAP = 0.02) and 6.2 at $v = 209$ km s^{-1}, period = 14.420 days (FAP = 0.04).

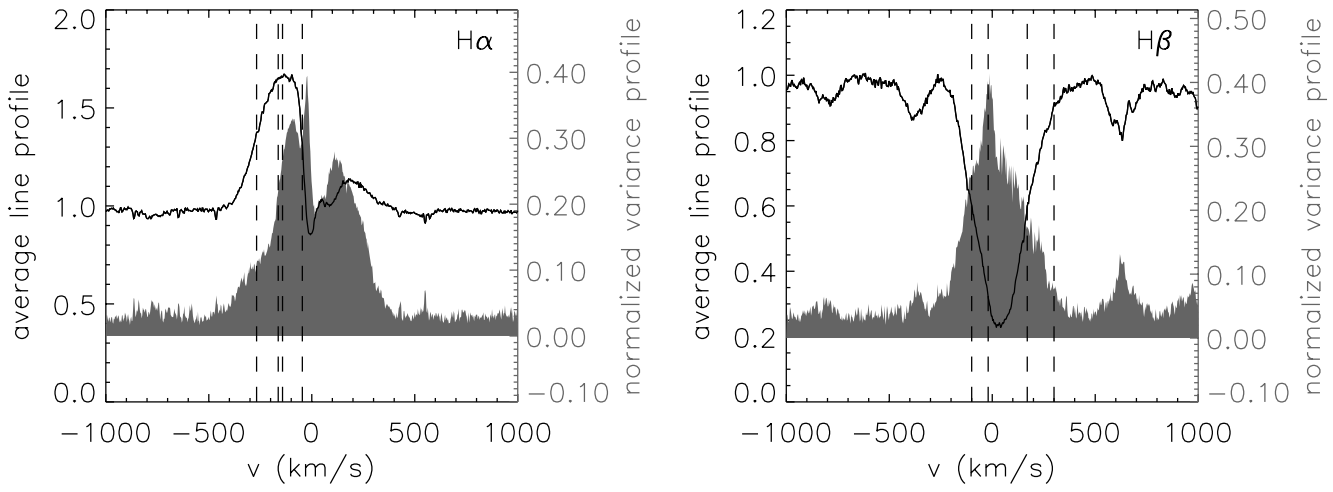

Fig. 10. Average Hα and Hβ line profiles (solid lines) and variance profiles (grey shaded areas) for the April/May 2000 run. The dashed lines indicate the profile regions that presented periodicities.

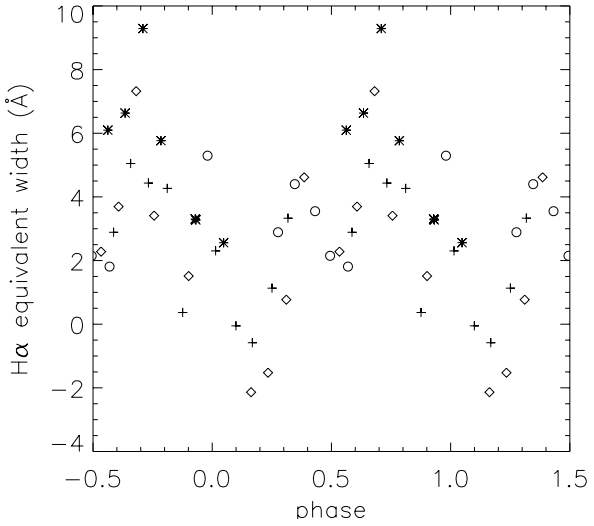

Fig. 11. Total Hα equivalent width folded at the orbital period. Different symbols refer to different orbital cycles. The crosses correspond to the 1998 observations and the other symbols to the 2000 ones. Negative values indicate that the line was mostly in absorption.

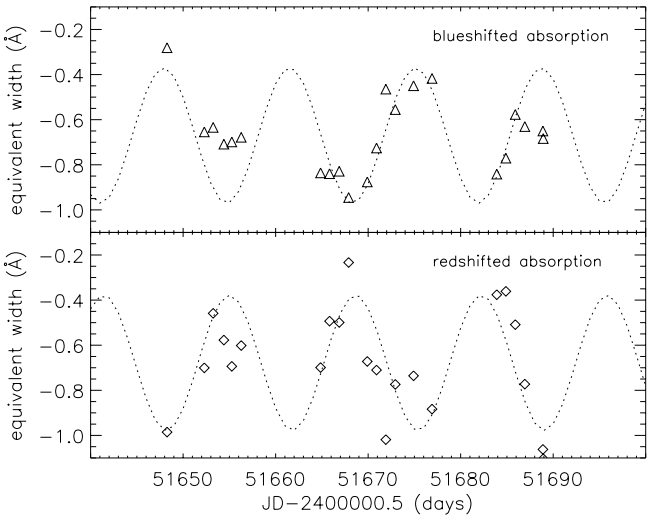

Fig. 12. Equivalent width variation of the two Hβ regions that presented the periodicities shown in Fig. 9. The blue and red regions vary almost 180° out of phase. The blueshifted region corresponds to -100 km s^{-1} $< v < -20$ km s^{-1}, the redshifted region to 150 km s^{-1} $< v <$ 340 km s^{-1}.

AK Sco consists of two F5 stars, and not much is known about convection, dynamos and magnetic fields in F stars in general. However, UV excesses associated with shock regions at the footprints of accretion columns have been measured for SU Aur (G2) (Gullbring et al. 2000) and CO Ori (F8) (Nuria Calvet, personal communication), showing that magnetospheric accretion seems to occur in F-G type stars as well as at later spectral types. The magnetosphere geometry that would allow for such an out-of-phase behavior inHβ in AK Sco is not obvious either. We do not know if there is a global magnetic field associated with the circumbinary disk, or if the magnetosphere of the two stars interact individually with the circumbinary disk and with each other as they approach at periastron.

5. Constraining the system parameters

The masses and radii of the stars in AK Sco are key parameters in any theoretical modeling of the system. Unfortunately, as no eclipses are observed, the orbital inclination and hence the absolute masses and radii cannot be determined directly. However, indirect evidence allows us to constrain the parameters within narrow ranges. Briefly, the absence of eclipses defines an upper limit to the inclination, hence a lower limit to the masses, while the distance from the Hipparcos parallax and the known luminosity and effective temperatures of the stars constrain the radii, as do the observed rotational velocities. To exploit these facts, we proceed as follows.

We assume that the de-reddened magnitude at maximum light ($V_0 = 8.28$) corresponds to the brightness of the non-obscured stars, fix their effective temperatures at 6500 K (as estimated by Andersen et al. 1989,from the spectral class), and use bolometric corrections for this temperature from Popper (1980). Adopting our spectroscopic orbital elements (Table 4), the size of the orbit and the stellar masses depend only on the orbital inclination, which we have varied from 85° to 60°, corresponding to a total binary mass of 2.14 $M_\odot$ to 3.26 $M_\odot$ respectively. We did not investigate lower inclinations, because the fit to the SED of AK Sco becomes poor for $M_A+M_B > 3\ M_\odot$ (see Sect. 6). As the masses and luminosities of the two stars are indistinguishable, we assume that also their radii are identical. A modified version of the WD light-curve synthesis program (Wilson & Devinney 1971; Wilson 1993; Vaz et al. 1995), combined with a set of scripts and programs developed by Vaz, was used to calculate the stellar and orbital parameters for each assumed inclination, using theoretical radial velocity curves identical to those observed. No attempt was made to model the non-periodic light variations in AK Sco (see Fig. 1).

Figure 14 summarizes our results. The dashed area is the region where eclipses would occur. The dashed line corresponds to the Hipparcos distance to the system ($D = 145$ pc). The solid horizontal lines indicate the range in stellar radii which satisfy the upper and lower 1σ distance limits defined by the Hipparcos parallax (145^{+38}_{-25} pc). The dotted line shows the radius of a star rotating synchronously at periastron passage with the observed $v \sin i$ (~18.5 km s^{-1}). At the Hipparcos distance (dashed line), the stars rotate faster than the expected synchronous rotation at periastron, in which case the stars would still be braking down. This is expected for PMS systems but is not always the rule: the primary of TY CrA, for example, seems to be highly subsynchronous (Casey et al. 1998).

In summary, the stellar radii should be below the dotted line, above the lower solid line and to the left of the dashed area in Fig. 14, although values between the dotted line and the upper solid line cannot be excluded. The corresponding radii and masses are significantly smaller and closer to the ZAMS values for F5 stars than those proposed by Andersen et al. (1989) who did not, however, have the Hipparcos parallax available to constrain the luminosity of the system. For inclinations within the acceptable range $65° < i < 70°$ we find the following mean physical parameters for these two near-identical stars: $M = 1.35 \pm 0.07\ M_\odot$, $R = 1.59 \pm 0.35\ R_\odot$, and $v \sin i = 18.5 \pm 1.0$ km s^{-1}.

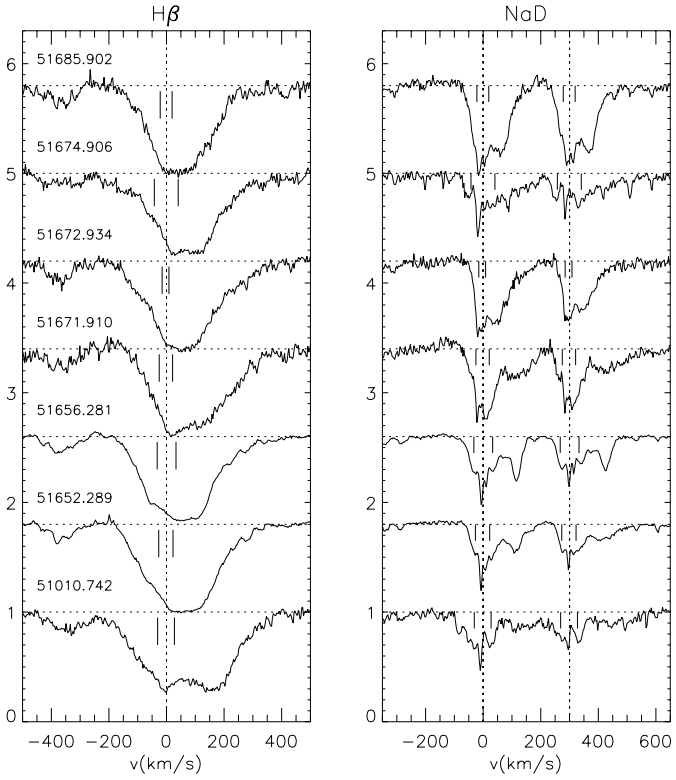

Fig. 13. Some particularly redshifted Hβ profiles and corresponding profiles for NaD. The horizontal dotted lines indicate the continuum position, the vertical dotted lines show the velocity of the system, and the short vertical solid lines correspond to the two stellar velocities. The highly redshifted components of the NaD lines clearly cannot be associated with the stars themselves. The numbers on the left are JD-2 400 000.0.

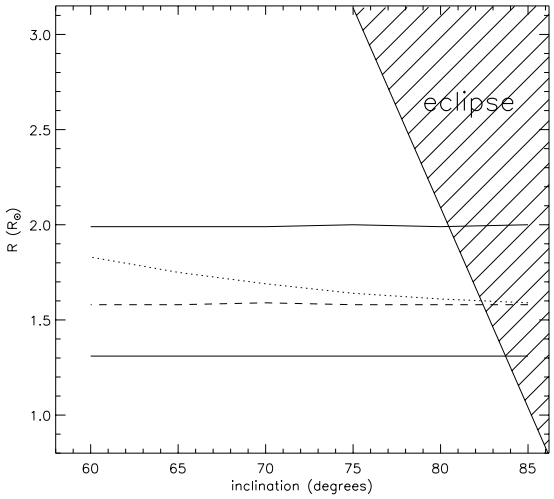

Fig. 14. Constraints on the parameter space of AK Sco. The dashed area shows the region where eclipses would occur; the dashed line corresponds to the Hipparcos distance to the system (D = 145 pc), and the solid horizontal lines indicate the constraints on the radii by the upper and lower Hipparcos distance limits. The dotted line corresponds to a stellar rotation at periastron passage equal to the measured $v \sin i$.

In order to check if our final parameters are consistent with those of a PMS star we calculated the luminosity of each component for the range of radii obtained in Fig. 14 and an assumed $T_{\rm eff} = 6500 \pm 100$ K. The $T_{\rm eff}$ and luminosities were then compared with the latest Palla & Stahler (2001) evolutionary tracks. Figure 15 shows that our luminosity and $T_{\rm eff}$ values correspond to stellar masses of 1.3–1.4 $M_\odot$ and ages of 10–30 Myr, consistent with our spectroscopic orbits for inclinations within the acceptable range $65° < i < 70°$.

AK Sco seems to be a member of the Upper Sco star formation region according to its distance ($D = 145^{+38}_{-25}$ pc), which is consistent with the derived Hipparcos distance to Upper Sco (de Zeeuw et al. 1999). The age of this star formation region was estimated by several authors and varies from 5 to 10 Myr (de Geus et al. 1989; Preibisch & Zinnecker 1999; Sartori et al. 2003; Preibisch et al. 2002), agreeing only marginally with the age we obtained for AK Sco using the Palla & Stahler (2001) evolutionary tracks. This discrepancy could in part be due to the methods used to calculate the birthline of evolutionary models, recently called into question by Hartmann (2003).

6. Disk models

6.1. Overall disk configuration

We have derived the spectral energy distribution (SED) of AK Sco from optical to millimeter wavelengths, using our own photometry and data from the following references: Andersen et al. (1989, *UBVRI*), Herbst et al. (1994, *UBVRI*), Kilkenny et al. (1985, *UBVRIJHKL*), Hutchinson et al. (1994, *BVRIJHKMNQ*), Jensen & Mathieu (1997, *JHKL*1*MNQ*, narrow band 10 μm filters), Weaver & Jones (1992, improved IRAS fluxes) and Jensen et al. (1996, 450, 800 and 1100 μm). At optical wavelengths, we chose the brightest available observations to represent the stellar SED, assuming that the light variations are mostly due variable extinction, as seems to be the case for AK Sco. At longer wavelengths there are much less data available, and the cause of the variations is much less clear: we have then adopted the mean value of the observations at wavelengths greater than 1 μm. The error bars at optical and near-infrared wavelengths correspond to the range of the available photometry, while the errors at other wavelengths are those of the individual measurements. Except in the optical, these errors could easily be underestimated due to undetected variability.

The visual extinction calculated from the brightest observations is $A_V = 0.5 \pm 0.1$, assumed to be interstellar rather than circumstellar in origin. We have therefore de-reddened the other fluxes from the optical to 250 μm using the Mathis (1990) interstellar reddening law and $R = 3.1$. Fluxes at wavelengths greater than 250 μm were not de-reddened, as the extinction at these wavelengths is almost negligible. Our de-reddened fluxes agree with those of Andersen et al. (1989).

Despite its relatively late spectral type of F5, AK Sco photometrically resembles the Herbig Ae/Be stars and has a total luminosity of 8.40 $L_\odot$. It also shows a near infrared bump in the SED, which is typical of Herbig Ae systems (Natta et al. 2001). For these reasons we decided to fit the SED of AK Sco with the disk model for Herbig Ae/Be stars by Dullemond et al. (2001, henceforth DDN01). This is a modified version of the Chiang & Goldreich (1997) flaring disk model, with the central disk

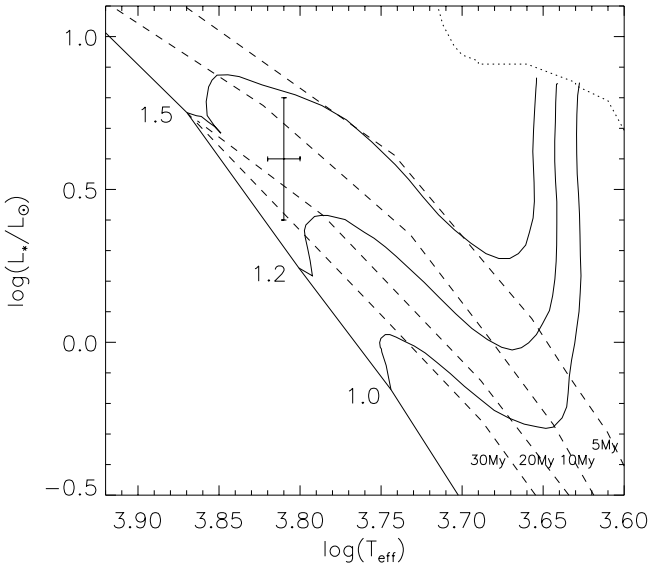

Fig. 15. Palla & Stahler (2001) evolutionary tracks (thick solid lines) labeled by the mass in solar units and isochrones (dashed lines) given in units of 10^6 yr. The dotted line is the birthline and the thin solid line represents the Main-Sequence. The observed luminosity and temperature of the mean component of AK Sco are shown as a cross. The luminosity errors are determined from the Hipparcos parallax; the temperature error corresponds to one spectral subclass (±100 K).

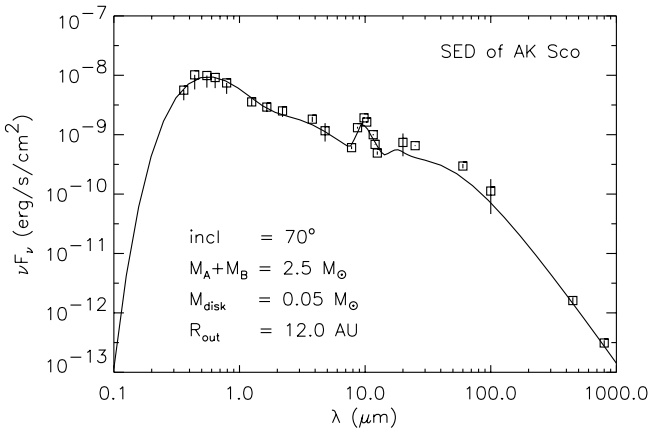

Fig. 16. Best model fit to the SED of AK Sco. The parameters used were $M_A + M_B = 2.5\ M_\odot$, $M_{disk} = 0.02\ M_\odot$, $R_{out} = 12$ AU, $i = 70°$, and constant surface density as a function of radius. The de-reddened photometric data are shown as squares and the fit as a solid line. The observational errors are discussed in the text and could be underestimated due to variability.

regions removed and a puffed-up inner rim included. The inner rim is hotter than the rest of the disk because it is directly exposed to the stellar flux. This rim is responsible for the near-infrared bump, while the rest of the disk produces the mid- and far-infrared emission. The main parameters of the model are the mass of the disk, the distribution of this mass within the disk, and the inner and outer disk radii. The disk models discussed here are all passive; i.e. they emit reprocessed stellar radiation only, with no additional luminosity generated by the accretion process itself.

In the original model of DDN01 the inner radius is fixed by assuming it to have the dust evaporation temperature of 1500 K. But dynamical effects could push this inner radius farther outwards, yielding a cooler rim and therefore a near infrared bump that is slightly shifted towards longer wavelengths. This is precisely what appears to be the case in AK Sco: instead of the usual inner-rim temperature of 1500 K, a temperature of 1250 K (at $R_{in} = 0.4$ AU) is required to fit the near-infrared bump. Since AK Sco has a projected semi-major orbital axis of $a \sin i = 0.143$ AU, thus occupying an appreciable fraction of the central gap, the tidal interaction of the binary with the circumbinary disk could plausibly cause that gap to be wider than expected. An exact theoretical prediction for this inner radius is difficult to give, but the simulations of Artymowicz & Lubow (1997) suggest that an eccentric binary like AK Sco will clear a gap in the circumbinary disk with a radius of about three times the orbital semi-major axis or about 0.43 AU for AK Sco, in good agreement with what we infer from the SED.

The strength of the near-infrared bump and the shape of the SED at longer wavelengths depend on the disk mass, the distribution of this mass, and the outer radius of the disk. There are a number of fine-tuning parameters in the model, related to the dust size distribution and the dust species, but these turn out to have a rather minor influence on the results. For the dust opacity we choose a mixture of 95% astronomical silicate grains of 0.1 μm and 5% graphite grains, also of 0.1 μm.

The best model has $R_{out} = 12$ AU, $M_{disk} = 0.02\ M_\odot$, and constant surface density as a function of radius. We assume a gas-to-dust ratio of 100. The SED computed for an inclination of $i = 70°$, consistent with the results of Sect. 5, is shown as a solid line in Fig. 16, where the stellar spectrum is approximated by a blackbody curve. It is clear that this model, although qualitatively good, slightly underpredicts the flux at all wavelengths up to 100 μm. We have found no set of parameters for which a higher infrared flux could be obtained, unless we reduced the total stellar mass to $M_* = 2\ M_\odot$, for which a very good fit is obtained. This happens because if the mass of the star is lowered, then the vertical gravity is lowered, so the disk is geometrically thicker and it covers a larger fraction of the sky of the star, capturing more stellar flux, which increases the predicted SED and therefore fits the measured SED better. However, our spectroscopic orbit only allows a minimum total mass of $M_* = 2.11\ M_\odot$ for an inclination of 90°. The maximum inclination that does not cause an obscuration of the stars by the disk is 78°, corresponding to a total mass of $M_* = 2.26\ M_\odot$.

Jensen & Mathieu (1997, hereafter JM97) obtained as good a fit to the SED of AK Sco as we, but within a different physical scenario. They used a geometrically thin disk with a power-law surface-density distribution and a hole to simulate disk clearing by the binary. In order to fit the AK Sco SED (more precisely the near-infrared and the silicate emission) they had to include $\sim 10^{-9}\ M_\odot$ of optically thin material inside the hole. Their result does not preclude a dynamically cleared region near the star, but indicates that there is some continued replenishment of the expected disk gap. They obtained a disk mass of $1.7 \times 10^{-3}\ M_\odot$, roughly 10 times smaller than our estimated disk mass.

This difference between the models is easy to explain. We have also tried optically thin disks at mm wavelengths and

obtained $M_{\rm disk} = 2 \times 10^{-3}\ M_{\odot}$, in agreement with JM97. In our best fit model, however, the disk is optically thick even at mm wavelengths. In this way, the interior of the disk may contain a lot of mass without having it show up at mm wavelengths. This model corresponds to a more massive disk with $M_{\rm disk} = 2 \times 10^{-2}\ M_{\odot}$ and in order to become optically thick, the disk then has to be very small ($R_{\rm out} = 12$ AU). A similar effect is found for Herbig Ae/Be stars having a comparatively weak far-IR excess (group II sources, in the terminology of Meeus et al. 2001). By fitting these sources with the DDN01 model, Dominik et al. (2003) found parameters representing small, massive and mostly optically thick disks, just as our fit for AK Sco. However, it is known from CO submillimeter mapping that Herbig Ae/Be disks can in some cases be much larger than that. The reason for this apparent paradox is still unknown.

Based on the SED alone, it is difficult to distinguish between the models of DDN01 and JM97 and decide if the disk is optically thin or thick at mm wavelengths and whether the near infrared emission comes from material in the cleared region or from the inner edge of the circumbinary disk. This is not totally unexpected since the physical state of disks, especially in binaries, is not yet well understood. Optically thin material in the gap would certainly contribute to the SED and is in part needed to explain the ongoing accretion process in AK Sco. However, even the small optically thick disk should be resolvable with the large submillimeter array ALMA now under construction in Chile, so it may become possible to settle the issue in the relatively near future.

One may speculate whether the contribution of this optically thin material is energetically significant. For it to contribute significantly to the SED the dust particles would have to cover a significant portion of the sky around the binary so as to create the bump in the SED around 4 μm. In order to estimate the portion of the total flux emitted around 4 μm, we subtracted the stellar contribution from the SED and fitted a blackbody curve of $T = 1250$ K to the 4 μm bump part of the SED. This blackbody fit contains 60% of the total flux of the disk, corresponding to 18% of the stellar luminosity. This means that the material emitting this part of the SED must cover at least 18% of the sky seen from the two central stars. That may be difficult to achieve with optically thin material alone. Considering that this part of the SED accounts for 60% of the total disk flux, the matter responsible for the 4 μm flux is in fact a dominant contributor to the SED of the disk and we would not expect this to be a small amount of matter flowing through the gap.

If one gives up the assumption that the matter needs to be optically thin, one may be able to explain this strong contribution. But then the question naturally arises if this contribution is not just the disk itself that reaches through the gap, instead of a small amount of matter within the cleared-out gap. Following this possibility one can try to determine the temperature of the optically thick matter inside the gap, which must be around 1250 K, which automatically gives back the inner radius of this large bulk of matter. In the optically thick case we are then almost naturally back at the disk and inner rim scenario.

One way to investigate the presence of material within the circumbinary gap would be through the detection of CO fundamental emission, for there the line profiles provide kinematic information which allows positioning the emitting material. In a recent paper on the PMS binary DQ Tau, Carr et al. (2001) showed that the width of the CO lines strongly indicate that the emission is coming from inside the disk gap rather than the circumbinary disk atmosphere in Keplerian rotation. Similar results were also obtained for the binary systems UZ Tau E and GW Ori (Mathieu, studies in progress) and such an investigation of AK Sco would be very important.

We should finally remember that there may well be a contribution to the SED due to accretion which is not included in our passive disk models. We do not know the accretion rate of AK Sco and we are not aware of any measurements of it, but assuming $M_{\rm acc} = 10^{-8}\ M_{\odot}\,{\rm yr}^{-1}$, the viscous energy release by active accretion contributes negligibly to the SED. It may, however, change the temperature of the disk in the midplane, thereby modifying the geometry of the disk somewhat. This, in turn, may affect the shape of the SED. We have verified that for a viscosity parameter α less than 10^{-4}, this effect does not significantly modify our model results.

We note that neither our disk scenario nor that of JM97 is able to reproduce exactly the height of the silicate emission feature, so something is probably still missing in them. They could also both be basically correct but just incomplete, and the near infrared emission could come from the circumbinary inner edge and also from some optically thin material in the cleared region.

6.2. Small scale structure in the disk

Assuming that all the brightness decreases of AK Sco from maximum are due to non-uniform dust obscuration in front of the two stars, the photometry will give the total absorption while a simultaneous CCF equivalent width ratio will give its distribution between the two stars. We may therefore calculate the dust extinction in front of each component at each point of the orbit using the subset of the simultaneous *uvby* photometry and CORAVEL observations, which cover nearly two full orbital cycles separated by four years (photometry data sets 1989*a* and 1993) plus a few scattered additional points. The results are shown in Fig. 17. There are clear variations from cycle to cycle, and in general the largest absorption is in front of the nearest of the two stars, as expected if the dust clumps are located preferentially in a circumbinary disk instead of inside the binary orbit, in agreement with the results of Fig. 7. Some exceptions are seen in Fig. 17, however, when the greatest absorption occurs in front of the more distant star, indicating the presence of dust clumps/clouds inside the binary orbit or entirely out of the disk plane. These conclusions are reinforced by the full CORAVEL data set, which yields a value for the luminosity ratio at *every* observation, even when non-photometric conditions prevented us from determining the total extinction to the system at the same time.

It is remarkable that the dust obscuration in front of an individual star in AK Sco may change significantly over a projected distance of just a single stellar diameter (~3–4 $R_{\odot}$), indicating that substructure in the disk or cloud exists at such small scales.

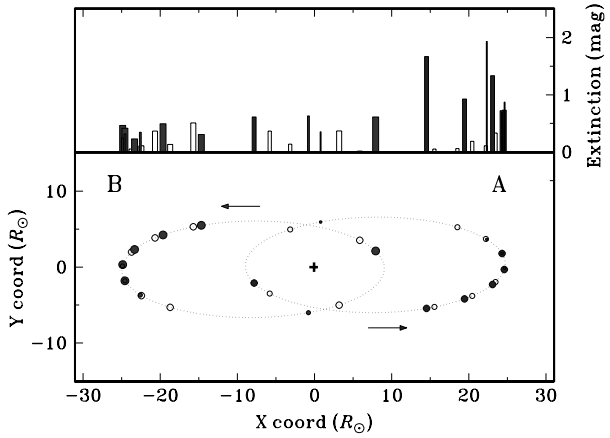

Fig. 17. Optical dust extinction at points along the binary orbit as determined from simultaneous photometry and spectroscopy over two orbital cycles in 1989 and 1993. The lower panel shows the two orbits in physical units and the position of both stars at each observed point (open and filled symbols indicating the 1989 and 1993 cycles, respectively); the direction of the orbital motion is indicated. The major axis of the orbit is in the plane of the sky; the orbit is shown face-on, but the *XY* plane is actually observed under the poorly-determined inclination angle *i*. At each instant the two stars are located at symmetric locations in their orbits, and we know which one is in front (i.e. at negative *Y* coordinates). The upper bar plot shows the extinction in magnitudes for each star at each point, empty and filled bars referring to the 1989 and 1993 data (bars for star A wider than those for star B). Thin bars indicate a few scattered additional observations (see the electronic version of the paper for a color coded version of this figure).

It is perhaps even more remarkable that the dust is obviously not symmetrically disposed around the binary orbit, as star A suffers significantly more obscuration near apastron than star B when they are located at opposite extremes of the orbit, at least when our 1993 observations were obtained. Thus, the "lower, right-hand" part of the disk in Fig. 17 (the true orientation of the figure on the sky is, of course, unknown) obscures star A most strongly at phases 0.2–0.5, resulting in $H_B/H_A > 1$; if this part of the disk is not only denser but also more clumpy, H_B/H_A would also show stronger scatter at these phases, as indeed observed (cf. Fig. 7).

7. Discussion

In the previous sections we saw that the AK Sco binary orbit governs accretion and outflow related features such as red and blue regions of the wide Hβ profile and the Hα equivalent widths. This might indicate that the magnetic field structure of the system (if accretion goes through magnetic field lines in F5 stars) is deeply related to the orbital motion. Another possibility is that there are accretion flows in the system from the circumbinary disk to the stars, perhaps as suggested by Artymowicz & Lubow (1996). As the stars orbit each other they are constantly presenting to us a different geometric perspective on those flows, both in the gap itself and as the gas flows meet the stellar magnetospheres and slide down along their local magnetic field lines, producing the observed emission lines. This could naturally result in an orbital periodicity in the line profiles if the accretion lines thus formed are modulated by gas and dust orbiting the system. The magnetic fields are not necessarily related to the orbital motion in this particular scenario.

Not much is currently known about the existence of magnetospheres in mid-F stars. There is compelling evidence that lower-mass T Tauri stars have an overall dipole field structure that governs the accretion process (Johns-Krull & Valenti 2000), but the physical scenario for F stars is still very uncertain. Some UV excesses associated to accretion shock regions have been measured for SU Aur (G2) (Gullbring et al. 2000) and CO Ori (F8) (Nuria Calvet, personal communication) showing that magnetospheric accretion may be going on in F-G type stars as well. According to the magnetospheric accretion scenario (Shu et al. 1994), if circumstellar disks were present in AK Sco they would likely be truncated near the star/disk co-rotation point, which can be regarded as a lower limit for the size of the stellar magnetosphere. However, in AK Sco the stars approach each other too closely at periastron (~15 $R_\odot$ or 10 stellar radii) for circumstellar disks to survive and be considered the source of accreted material. Therefore the stars are expected to be tidally synchronized rather than disk locked.

The fact that we needed a circumbinary disk with a substantial gap to fit the SED does not preclude the existence of gas inside the gap to power accretion, but only indicates an optically thin inner region. Some level of replenishment of the inner circumbinary disk region is still necessary in AK Sco to explain the accretion related lines. The replenishment mechanism proposed by Artymowicz & Lubow (1996) may apply in part to AK Sco except that we do not see the accretion outbursts near periastron passage predicted for eccentric binaries with mass ratio close to one. Instead, we observe Hα equivalent width variations that are smooth with an amplitude of more than 3 times the mean value (Fig. 11), and which look rather like the mass accretion rate variations predicted by Artymowicz & Lubow (1996) for *low* eccentricity systems with unequal components (see their Fig. 2 – top panel), which is rather puzzling.

The orbital motion was also shown to be roughly related to the variability of the luminosity ratio between the two stellar components, probably due to dust clumps in the disk because the components have almost equal masses and are supposedly coeval. Once again, most of the variability occurs near phases 0.3–0.5, while phases near periastron present the least scatter.

Another intriguing result is related to the variable circumstellar extinction, which one would like to connect to the disk. However, at our favored inclination range ($65° < i < 70°$) the modeled disk does not obscure the central binary. Obscuration by the disk would only begin for $i > 78°$, but then at $i > 80°$ eclipses by the stars themselves are predicted and we do not observe them. This indicates that the real disk must be more turbulent and clumpy than the adopted model, which is an interesting but still idealized view of a young circumbinary disk. Tidal forces of the binary system, for example, could be responsible for perturbations near the disk inner boundary, moving material out of the disk upper surface, and thus creating some obscuring clumpy structure near the disk inner edge. Remarkably, our 1993 simultaneous data indicate that (at least the inner,

obscuring part of) the disk was not axially symmetric around the binary at that time.

Another possible circumstellar scenario for the system would be of an optically thin circumstellar envelope added to a geometrically thin and optically thick circumbinary disk (see Miroshnichenko et al. 1999). In that case the inhomogeneities that cause the photometric variability could be out of the disk plane and be part of the envelope itself. But then the "optically thin" envelope must still allow for enough dust extinction to dim the whole system by a magnitude and a half at times. It is still very difficult to distinguish between the two scenarios from the SED fit only (see Chiang et al. 2001, for a recent discussion). For most of the spectroscopic observations we have no simultaneous photometry. However, since our photometry shows no sign of any periodicity, it is not expected to correlate with the periodic spectroscopic variations.

Although young binary systems are expected to be much more complex than single stars, they often seem to show much of the same signs of accretion, meaning that somehow the star/disk interaction is not extremely affected by the binarity of the system, which is rather surprising. Like the results for DQ Tau (Basri et al. 1997), our data seem to imply that the accretion related line profiles do not depend on the formation of a well-organized circumstellar disk structure. It is also interesting to note that AK Sco is composed of two F5 stars which show many of the same signs of accretion as typical CTTSs.

8. Conclusions

We have analysed 32 échelle spectra of the PMS binary system AK Sco observed during 1998 and 2000, as well as 72 photoelectric radial-velocity observations from 1986 to 1994. These data allow considerable improvement of the period and other orbital parameters of the system. We have also analysed 8 sets of photometric observations from 1987, 1989, 1990, 1992, 1994 and 1997.

We detected no signs of any eclipses in the photometry, which is dominated by large, non-periodic variations of up to one magnitude from night to night. However, the well-determined Hipparcos parallax allows us to constrain the orbital inclination to $65° < i < 70°$, leading to the following mean physical parameters for these two near-identical stars: $M = 1.35 \pm 0.07\ M_\odot$, $R = 1.59 \pm 0.35\ R_\odot$, and $v \sin i = 18.5 \pm 1.0\ \mathrm{km\,s^{-1}}$.

We have successfully fitted a set of passive disk models to the SED of AK Sco, respecting the above parameter ranges. The disk models place the inner rim at an usually large distance from the stars, and we speculate that dynamical effects due to tidal interactions of the binary system are responsible for pushing the disk inner radius outwards. At our adopted inclination range the stars are not obscured by the model disk, which thus needs to be more clumpy and turbulent than predicted in order to explain the variable circumstellar extinction seen in the photometry. Moreover, our detailed 1993 extinction data appear to indicate significant asymmetries in the inner part of the disk at that time. Future sub-mm interferometric observations with high spatial resolution may give valuable additional constraints on the several different models which are obtained from the SED fit alone.

AK Sco shows emission and absorption lines that vary substantially. The accretion-related lines may show both infall and outflow signatures and resemble those observed in T Tauri stars. The system displays variations at the binary orbital period in both the photospheric and accretion-related line intensities and equivalent widths, although with appreciable scatter.

In AK Sco, we see no signs of enhanced accretion near periastron, as expected theoretically for binary systems with high eccentricity and nearly equal components. Instead, the Hα equivalent width displays rather smooth variations at the stellar period, peaking around phases 0.6–0.7 – indeed just when the stars are *farthest* apart. Clearly, much remains to be learned about accretion from circumbinary disks.

Acknowledgements. This research is based on data collected at the ESO 1.52-m telescope at La Silla, partly operated by the Observatório Nacional-CNPq as a result of the Brazilian-ESO agreement, and at the 0.5-m and 1.54-m Danish telescopes at ESO, La Silla, Chile. We thank the observers at the Geneva 70-cm photometric telescope at ESO La Silla, G. Burki, N. Cramer and B. Nicolet for the careful reduction of these data, and G. Burki for permission to analyse them in this paper and include them in Table 3. S.H.P.A. acknowledges support from FAPESP (grant number 00/06244-9) and CAPES (PRODOC program), J.A. acknowledges support from the Danish Natural Science Research Council and the Carlsberg Foundation and L.P.R.V. acknowledges support from the Brazilian Institutions CNPq and FAPEMIG. We thank Dr. Inge Heyer, STScI, for permission to include her unpublished 1989 *uvby* photometry in this study.

References

Allain, S., Queloz, D., Bouvier, J., Mermilliod, J. C., & Mayor, M. 1997, Mem. Soc. Astron. It., 68, 899
Andersen, J., Lindgren, H., Hazen, M. L., & Mayor, M. 1989, A&A, 219, 142
Artymowicz, P., & Lubow, S. H. 1994, ApJ, 421, 651
Artymowicz, P., & Lubow, S. H. 1996, ApJ, 467, L77
Baranne, A., Mayor, M., & Poncet, J. L. 1979, Vis. Astron., 23, 279
Baranne, A., Queloz, D., Mayor, M., et al. 1996, A&AS, 119, 373
Basri, G., Johns-Krull, C. M., & Mathieu, R. D. 1997, AJ, 114, 781
Bibo, E. A., & Thé, P. S. 1991, A&AS, 89, 319
Bouvier, J., Cabrit, S., Fernandez, M., Martin, E. L., & Matthews, J. M. 1993, A&A, 272, 176
Bouvier, J. 1997, Mem. Soc. Astron. It., 68, 881
Bouvier, J., Forestini, M., & Allain, S. 1997, A&A, 326, 1023
Burnet, M., & Rufener, F. 1979, A&AS, 74, 54
Carr, J. S., Mathieu, R. D., & Najita, J. R. 2001, ApJ, 551, 454
Casey, B. W., Mathieu, R. D., Vaz, L. P. R., Andersen, J. & Suntzeff, N. B. 1998, AJ, 115, 1617
Chiang, E. I., & Goldreich, P. 1997, ApJ, 490, 368
Chiang, E. I., Joung, M. K., Creech-Eakman, M. J., et al. 2001, ApJ, 547, 1077
Covino, E., Melo, C., Alcalá, J. M., et al. 2001, A&A, 375, 130
de Geus, E. J., de Zeeuw, P. T., & Lub, J. 1989, A&A, 216, 44
de Zeeuw, P. T., Hoogerwerf, R., de Bruijne, J. H. J., Brown, A. G. A., & Blaauw, A. 1999, AJ, 117, 354
Dominik, C., Dullemond, C. P., Waters, L. B. F. M., & Walch, S. 2003, A&A, submitted
Dullemond, C. P., Dominik, C., & Natta, A. 2001, ApJ, 560, 957
Edwards, S., Strom, S. E., Hartigan, P., et al. 1993, AJ, 106, 372

Etzel, P. B. 1985, SBOP – Spectroscopic Binary Orbit Program, Program Manual, UCLA
Golay, M. 1980, Vist. Astron., 24, 141
Gray, D. F. 1976, The observation and analysis of stellar photospheres (New York, Wiley-Interscience)
Gullbring, E., Calvet, N., Muzerolle, J., & Hartmann, L. 2000, ApJ, 544, 927
Hartmann, L. 1998, Accretion Processes in Star Formation (Cambridge University Press), Cambridge Astrophysics Series, 32
Hartmann, L. 2003, ApJ, 585, 398
Herbig, G. H., & Rao, N. K. 1972, ApJ, 174, 401
Herbst, W., Herbst, D. K., Grossman, E. J., & Weinstein, D. 1994, AJ, 108, 1906
Horne, J. H., & Baliunas, S. L. 1986, ApJ, 302, 757
Hutchinson, M. G., Albinson, J. S., Barrett, P., et al. 1994, A&A, 285, 883
Jensen, E. L. N., Mathieu, R. D., & Fuller, G. A. 1996, ApJ, 458, 312
Jensen, E. L. N., & Mathieu, R. D. 1997, AJ, 114, 301
Johns, C. M., & Basri, G. 1995a, AJ, 109, 2800
Johns, C. M., & Basri, G. 1995b, ApJ, 449, 341
Johns-Krull, C. M., & Valenti, J. A. 2000, Stellar Clusters and Associations: Convection, Rotation, and Dynamos, ASP Conf. Ser., 198, 371
Kaufer, A., & Pasquini, L. 1998, Proc. SPIE, 3355, 844
Kaufer, A., Stahl, O., Tubbesing, S., et al. 2000, Proc. SPIE, 4008, 459
Kilkenny, D., Whittet, D. C. B., Davies, J. K., et al. 1985, South African Astronomical Observatory Circular, 9, 55
Krist, J. E., Stapelfeldt, K. R., & Watson, A. M. 2002, ApJ, 570, 785
Mathieu, R. D. 1994, ARA&A, 32, 465
Mathieu, R. D., Stassun, K., Basri, G., et al. 1997, AJ, 113, 1841
Mathis, J. S. 1990, ARA&A, 28, 37
Meeus, G., Waters, L. B. F. M., Bouwman, J., et al. 2001, A&A, 365, 476
Melo, C., Pasquini, L., & De Medeiros, J. R. 2001, A&A, 375, 85
Miroshnichenko, A., Ivezić , Željko, Vinković, D., & Elitzur, M. 1999, ApJ, 520, L115
Natta, A., Prusti, T., Neri, R., et al. 2001, A&A, 371, 186
Nielsen, R. F., Nørregaard, P., & Olsen, E. H. 1987, ESO Messenger 50, 45
Palla, F., & Stahler, S. W. 2001, ApJ, 553, 299
Popper, D. M. 1980, ARA&A, 18, 175
Preibisch, T., & Zinnecker, H. 1999, AJ, 117, 2381
Preibisch, T., Brown, A. G. A., Bridges, T., Guenther, E., & Zinnecker, H. 2002, AJ, 124, 404
Queloz, D. 1995, Ph.D. Thesis 2788, University of Geneva
Queloz, D., Mayor, M., Naef, D., et al. 2000, From Extrasolar Planets to Cosmology: The VLT Opening Symposium, ed. J. Bergeron, & A. Renzini (Berlin: Springer-Verlag), 548
Rufener, F. 1964, Publ. Obs. Genève, A, 66, 413
Rufener, F. 1985, in Calibration of Fundamental Stellar Quantities, ed. D. S. Hayes, et al. (Dordrecht: Reidel Publ. Co.), IAU Symp., 111, 253
Santos, N., Mayor, M., Naef, D., et al. 2002, A&A, 392 215
Sartori, M. J., Lépine, J. R. D., & Dias, W. S. 2003, A&A, 404, 913
Scargle, J. D. 1982, ApJ, 263, 835
Shu, F., Najita, J., Ostriker, E., et al. 1994, ApJ, 429, 781
Vaz, L. P. R., Andersen, J., & Rabello Soares, M. C. A. 1995, A&A, 301, 693
Vaz, L. P. R., Andersen, J., Casey, B. W., et al. 1998, A&AS, 130, 245
Weaver, W. B., & Jones, G. 1992, ApJS, 78, 239
Wilson, R. E., & Devinney, E. J. 1971, ApJ, 166, 605
Wilson, R. E. 1993, Documentation of Eclipsing Binary Computer Model (revision of 1992 May, updated 1993 January)